Endoplasmic Reticulum Chaperone Glucose-Regulated Protein 94 Is Essential for Proinsulin Handling

Seyed Mojtaba Ghiasi,[1] Tina Dahlby,[1] Caroline Hede Andersen,[1] Leena Haataja,[2] Sólrun Petersen,[1] Muhmmad Omar-Hmeadi,[3] Mingyu Yang,[3] Celina Pihl,[1] Sophie Emilie Bresson,[1] Muhammad Saad Khilji,[1] Kristian Klindt,[1] Oana Cheta,[1] Marcelo J. Perone,[1,4] Björn Tyrberg,[5] Clara Prats,[6] Sebastian Barg,[3] Anders Tengholm,[3] Peter Arvan,[2] Thomas Mandrup-Poulsen,[1] and Michal Tomasz Marzec[1]

Diabetes 2019;68:747–760 | https://doi.org/10.2337/db18-0671

Although endoplasmic reticulum (ER) chaperone binding to mutant proinsulin has been reported, the role of protein chaperones in the handling of wild-type proinsulin is underinvestigated. Here, we have explored the importance of glucose-regulated protein 94 (GRP94), a prominent ER chaperone known to fold insulin-like growth factors, in proinsulin handling within β-cells. We found that GRP94 coimmunoprecipitated with proinsulin and that inhibition of GRP94 function and/or expression reduced glucose-dependent insulin secretion, shortened proinsulin half-life, and lowered intracellular proinsulin and insulin levels. This phenotype was accompanied by post-ER proinsulin misprocessing and higher numbers of enlarged insulin granules that contained amorphic material with reduced immunogold staining for mature insulin. Insulin granule exocytosis was accelerated twofold, but the secreted insulin had diminished bioactivity. Moreover, GRP94 knockdown or knockout in β-cells selectively activated protein kinase R–like endoplasmic reticulum kinase (PERK), without increasing apoptosis levels. Finally, GRP94 mRNA was overexpressed in islets from patients with type 2 diabetes. We conclude that GRP94 is a chaperone crucial for proinsulin handling and insulin secretion.

Type 2 diabetes (T2D) develops when pancreatic β-cell insulin secretion fails to compensate for increased insulin demands. Meeting those dynamic demands requires synthetic plasticity in β-cell production of proinsulin, a process periodically constituting up to 30–50% of total β-cell protein synthesis (1). Insulin is synthesized as a prepro-hormone (preproinsulin), the signal peptide of which is cleaved upon entering the endoplasmic reticulum (ER) to generate proinsulin (2). At this point, proinsulin monomer folding is initiated (3), and three intramolecular disulfide bonds are formed by protein disulfide isomerases (4). Subsequently, proinsulin dimerizes and is transported through the Golgi apparatus where it further assembles facilitated by zinc, calcium, and acidic pH. In secretory granules, proinsulin hexamers are cleaved by the endoproteases prohormone convertase 1/3 and 2 (PC1/3 and 2) to generate and store mature insulin (5). Despite intensive investigation, it remains unanswered how ER protein chaperones partake in this process (reviewed in Liu et al. [6]).

Glucose-regulated protein 94 (GRP94, gp96) is a paralog of an hsp90 chaperone abundantly expressed and localized to the lumen of the ER (7). GRP94 executes protein quality control (8) and folding of a limited clientele of proteins, including but not limited to β1 integrin (9), Toll-like receptors (10), and insulin-like growth factors 1 and 2 (IGF-1/2) (11). GRP94 is essential for growth and development of multicellular organisms (11,12) and is highly

[1]Department of Biomedical Sciences, University of Copenhagen, Copenhagen, Denmark
[2]Division of Metabolism, Endocrinology, & Diabetes, University of Michigan Medical Center, Ann Arbor, MI
[3]Department of Medical Cell Biology, Uppsala University, Uppsala, Sweden
[4]Instituto de Investigación en Biomedicina de Buenos Aires (IBioBA)-CONICET-Partner Institute of the Max Planck Society, Polo Científico Tecnológico, Buenos Aires, Argentina
[5]Translational Science, Cardiovascular, Renal and Metabolism, IMED Biotech Unit, AstraZeneca, Gothenburg, Sweden
[6]Center for Healthy Ageing, Department of Biomedical Sciences, University of Copenhagen, Copenhagen, Denmark

Corresponding author: Michal Tomasz Marzec, michal@sund.ku.dk

Received 15 June 2018 and accepted 26 December 2018

This article contains Supplementary Data online at http://diabetes.diabetesjournals.org/lookup/suppl/doi:10.2337/db18-0671/-/DC1.

S.M.G. and T.D. contributed equally to this work.

expressed in both exocrine and endocrine pancreas and bronchial epithelium due to their intense secretory function (13). GRP94 expression is upregulated in response to low glucose concentrations (12) and other metabolic stresses, e.g., hypoxia (14). Clientele restriction is reflected by the limited impact of GRP94 KD on ER stress, unfolded protein response (UPR) (15), and Ca^{2+} homeostasis (16), all critical aspects of β-cell biology. GRP94 ATPase activity (17) is inhibited by geldanamycin (18) or newly developed GRP94-specific inhibitors (19). Recently, GRP94 has been ablated in pancreatic and duodenal homeobox 1 (Pdx1)-expressing cells and shown to be an essential regulator of β-cell development, mass, and function (20).

GRP94 is critically involved in IGF-1/2 folding (11), and given that proinsulin and pro-IGFs share evolutionary origin and >50% amino acid homology and have highly similar tertiary structures (21), we hypothesized that GRP94 plays a critical role in proinsulin handling. We demonstrate that GRP94 coprecipitates with proinsulin and that knockout (KO), knockdown (KD), or pharmacological inhibition of GRP94 in insulin-producing cells or human islet cells results in a shortened proinsulin half-life, leading to lower intracellular proinsulin and insulin levels and reduced glucose-stimulated secretion of mature insulin. Additionally, we observe post-ER proinsulin misprocessing and generation of a high number of secretory granules containing amorphic material and less mature, bioactive insulin. Finally, GRP94 mRNA was overexpressed in β-cells in human islets from patients with T2D, likely as a compensatory response.

RESEARCH DESIGN AND METHODS

Cell Culture

The rat insulinoma INS-1E, GRINCH (INS-1 cells stably expressing hProCpepSfGFP) (22), and MIN6 cell lines were grown in RPMI-1640 or DMEM (Supplementary Data).

Generation of GRP94 CRISPR/Cas9–Mediated KO INS-1E Cell Lines

GRP94-KO INS-1E cells were generated using a ready-to-use lentiviral particle coding guide RNA (gRNA) sequence targeting rat *grp94* exon 3 or nontargeting gRNA (Supplementary Data).

Lentiviral shRNA–Mediated GRP94 KD

GRP94 was knocked down in INS-1E cell lines and dispersed human islets using pLKO.1 lentiviral shRNA particles and the Trans-Lentiviral shRNA Packaging System (Dharmacon, Søborg, Denmark) against GRP94 mRNA along with a nonsilencing shRNA according to the manufacturer's instructions (Supplementary Data).

Real-time Quantitative RT-PCR

The relative mRNA level of ER stress markers and insulin genes was determined by quantitative RT-PCR using specific primers (23) (Supplementary Table 1 and Supplementary Data).

Glucose-Stimulated Insulin Secretion

INS-1E cell lines (control or GRP94 KD or KO) or dispersed human islet cells after lentiviral transduction were examined for insulin secretion in response to 2 and 20 mmol/L glucose according to standard protocols (Supplementary Data).

Immunoprecipitation and Immunoblotting

Coimmunoprecipitation of GRP94 and proinsulin was performed using GFP-Trap_MA beads, and GRP94, GFP, and insulin proteins were detected in precipitates of whole cells using specific antibodies with immunoblotting (Supplementary Data).

Apoptosis and Cell Viability Assays

Apoptosis was assayed by detection of DNA/histone complexes released from the nucleus using a Roche cell death assay kit (Roche, Mannheim, Germany) according to the manufacturer's protocol. Cell viability was measured by alamarBlue assay (Life Technologies, Taastrup, Denmark) (Supplementary Data).

Electron Microscopy

Cells were grown to confluence, fixed, and embedded in epon. Sections were cut, stained with uranyl acetate and lead citrate or immunogold labeled using anti-insulin–specific antibody, and subsequently examined with a Philips CM100 transmission electron microscope. Manually marked secretory granules were analyzed with ZenLE software (Supplementary Data).

Confocal Imaging of INS-1E and GRINCH Cells

Cells were grown on coverslips and immune labeled with proinsulin-specific antibody (GS-9A8). Samples were imaged on a confocal Zeiss LSM710 microscope through a Plan-Apochromat 63×/1.4 and analyzed using the Zeiss Zen software (Supplementary Data).

Recordings of Secretory Granule Exocytosis and Insulin Action

Stimulated exocytosis of secretory granules and autocrine insulin action were evaluated with total internal reflection fluorescence (TIRF) microscopy of INS-1E, MIN6 cells, and human islets expressing either the granule marker neuropeptide-Y (NPY)-GFP or the PIP3 reporter GFP4-GRP1 and pretreated with GRP94 inhibitor (GRP94i) (Supplementary Data).

Single-Cell RNA Sequencing of Pancreatic Islets

Gene expression in islet cell subtypes was determined by reanalyzing published human islet single-cell sequencing data (EBI: MTAB-5061) (24) (Supplementary Data).

In Silico Modeling of Protein Interactions

Using ZDOCK 3.0.2 modeling software, prediction models of interactions between GRP94 (5ULS, 2O1U, and 2O1V) and either proinsulin (2KQP) or IGF-I (1IMX) were generated based on crystal structures from the protein data bank (25) (Supplementary Data).

Metabolic Labeling

INS-1E cells were labeled for 1 h with ^{35}S-Met/Cys and chased for 1 h. Cell lysates, normalized to trichloroacetic acid–precipitable counts, were immunoprecipitated with anti-insulin antibodies and then analyzed by SDS-PAGE and phosphorimaging (Supplementary Data).

Statistics

Differences between two groups were assessed by Bonferroni-corrected two-tailed Student *t* test or by ANOVA for multigroup comparisons with post hoc Student *t* tests corrected for multiple comparisons using GraphPad Prism version 6 (La Jolla, CA). Data are presented as means ± SD or SEM. *P* values ≤0.05 were considered significant.

RESULTS

GRP94 Interacts With Proinsulin

Pro-IGF1/2 and proinsulin share >50% amino acid homology and have similar tertiary structures (21), and since GRP94 presence and activity are essential for proper IGF1/2 folding and maturation (26), we investigated whether GRP94 might possess proinsulin folding properties. Using ZDOCK modeling software and crystal structures of GRP94 (5ULS, 2O1U, and 2O1V) and proinsulin (2KQP), we generated models of their interaction suggesting that proinsulin (purple) can bind to a GRP94 homodimer (green/blue) client binding site (CBS; amino acids 652–676) (Fig. 1*A*, top models presented) (GRP94–IGF-1 model, Supplementary Fig. 1*A*–*C*) and extends outwards of the complex (5ULS and 2O1V) or toward the GRP94 N-terminal domain (2O1U). Residues 73–83 in proinsulin chain A were predicted to interact with GRP94 CBS (Supplementary Table 3), but the GRP94-proinsulin interaction did not involve proinsulin cysteines.

We confirmed a GRP94-proinsulin interaction by immunoprecipitating exogenously expressed GFP-tagged GRP94 from INS-1E cells, or GFP-tagged proinsulin (hPro-CpepSfGFP) from GRINCH cells, followed by Western blotting (WB) analysis showing bidirectional coprecipitation of GRP94 and proinsulin (Fig. 1*B* and *C* and Supplementary Fig. 1*B*).

GRP94 KD or KO Does Not Lead to β-Cell Death but Induces ER Stress via the PERK Pathway

We performed lentiviral shRNA KD or CRISPR/Cas9-induced KO to examine the effects of GRP94 ablation in INS-1E cells (Fig. 2*A* and Supplementary Figs. 2–5). Compared with the control, no statistically significant increase in apoptosis was observed in GRP94 KO and KD cells (Fig. 2*B* and Supplementary Fig. 5, showing apoptosis rate vs. KD and KO respective controls). Treatment for 24 h with 1 μmol/L of thapsigargin induced apoptosis 4- to 10-fold in control INS-1E cells.

We next examined the activation of the UPR pathways in the GRP94 KD cells. ATF4 and CHOP mRNAs were significantly upregulated, suggesting protein kinase R–like endoplasmic reticulum kinase (PERK) activation (27), with no changes in the levels of spliced or unspliced XBP1 (Fig. 2*C*) and no effect on the expression of non-related genes or total protein level (Supplementary Figs. 3 and 4). ER stress has been reported to induce Ins-1/2 mRNA degradation through regulated Ire1α-dependent decay (RIDD) (28), but Ins-1/2 mRNA levels were not significantly lower in GRP94 KD cells. We evaluated RIDD activity in GRP94 KD cells with or without 30 μmol/L Ire1α inhibitor 4q8C. This led to a complete block of Ire1α-dependent XBP1 splicing in both KD and control cells but did not result in an upregulation of Ins-1/2 mRNA levels (Fig. 2*C*).

Diminished Intracellular Proinsulin and Insulin Contents After GRP94 KD, KO, or Pharmacological Inhibition

We next investigated the impact of GRP94 KD and KO on proinsulin and insulin intracellular levels. GRP94 KD and, to a greater extent, GRP94 KO cells showed a significant reduction in proinsulin contents (45–70%), as evidenced by WB and ELISA analysis (Fig. 3*A* and *B*). Similarly, insulin levels were reduced (20–45%), reaching statistical significance in GRP94 KO cells. In response to the shift in glucose concentration from 2 to 20 mmol/L, GRP94 KD/KO and control cells upregulated intracellular levels of proinsulin (two- to fourfold) and insulin (onefold) (Supplementary Fig. 6) starting from normal (control) or low (GRP94KD/KO) expression levels (Fig. 3*A*).

Next, we used PU-WS13, a selective GRP94i (19), to acutely inhibit GRP94 ATPase activity. Cells were pretreated for 4 h with 5 or 20 μmol/L of the inhibitor in 2 or 20 mmol/L glucose–containing media. No loss in cell viability was observed even after 24-h treatment with 20 μmol/L of GRP94i (Supplementary Fig. 7). Inhibition of GRP94 ATPase activity significantly diminished the cell contents of proinsulin and insulin as analyzed by WB (quantification of n = 6) (Fig. 3*C*), indicating that the proinsulin chaperoning function of GRP94 is energy requiring. Similar results were obtained with human islets exposed to 20 μmol/L of GRP94i for 4 h (n = 2) (Fig. 3*D*).

GRP94-Deficient Cells Exhibit Diminished, Non–ER-Localized Proinsulin Accompanied by an Increased Number of Secretory Granules With Amorphic Content and Lower Immunogold Staining for Mature Insulin

We immunostained for proinsulin with GS-9A8 antibody and observed a nuclear and a cytoplasmic granular staining signal distribution in control cells (juxtanuclear Golgi region) (22), but a much more diminished and diffused, non–ER-localized stain in GRP94 KD cells (Fig. 4*A*). GRINCH cells expressing hProCpepSfGFP had the GFP signal localized within the ER, Golgi, and secretory granules and aligned along subplasmalemmal regions (22) (Fig. 4*B*). However, upon GRP94 KD, the GFP signal was substantially diminished, particularly at the subplasmalemmal regions (Fig. 4*B*).

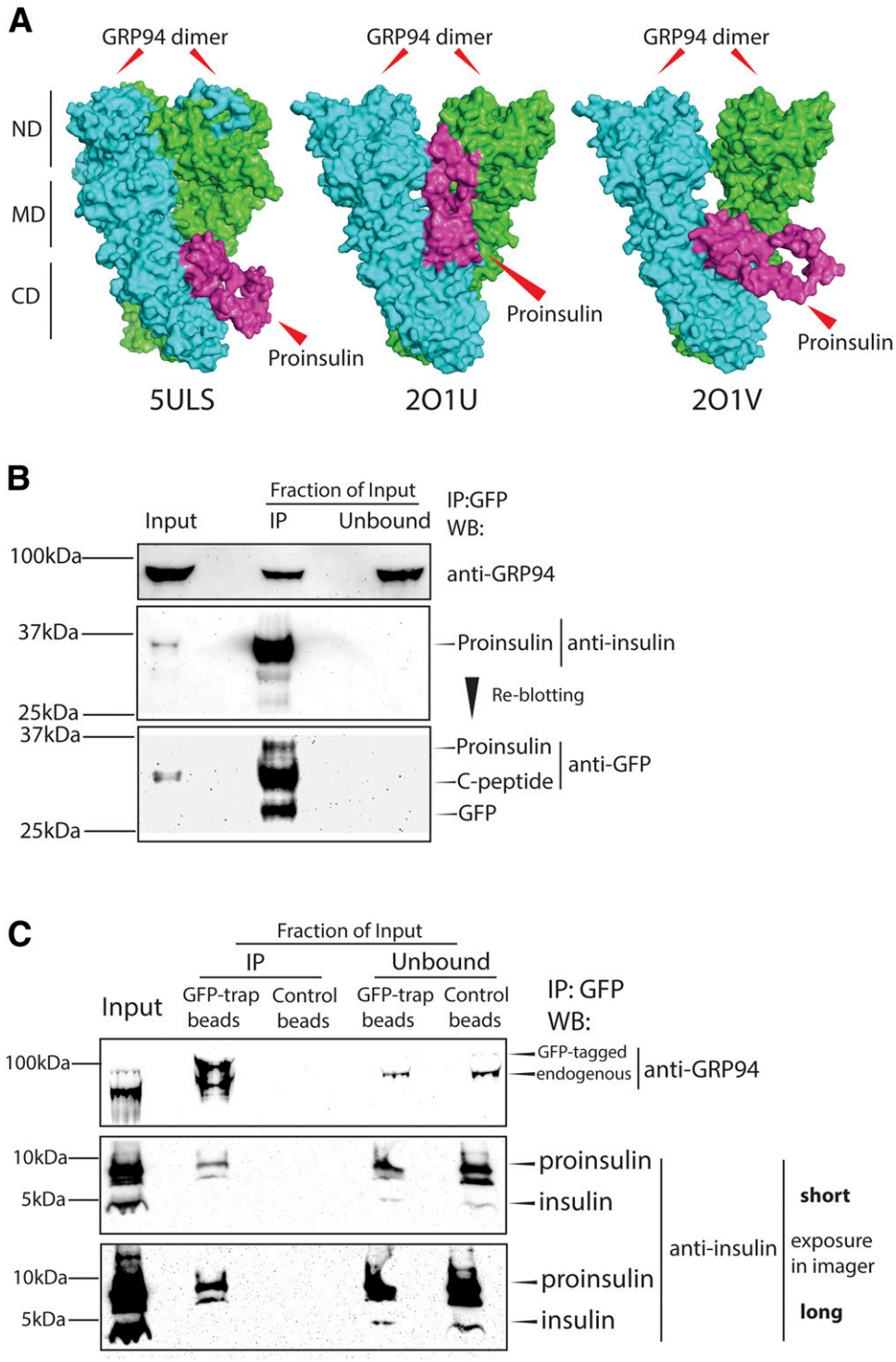

Figure 1—GRP94 interacts with proinsulin. *A*: GRP94-proinsulin interaction was analyzed in silico by the docking computational modeling software (ZDOCK 3.0.2) with proinsulin (2KQP, purple) and three GRP94 crystal structures: one open (5ULS) and two closed (2O1U and 2O1V, all green/blue). The top-scored prediction model of each pair is presented. CD, C-terminal domain; MD, middle domain; ND, N-terminal domain. Next, binding of GRP94 to proinsulin was tested in *B*. *C*: GRINCH cells (INS-1 cells stably expressing hPro-CpepSfGFP) and INS-1E cells expressing GFP-tagged GRP94. Cells were lysed, and GRP94 (INS-1E) or proinsulin (GRINCH) was subjected to immunoprecipitation (via GFP-tag) and analyzed by SDS-PAGE and WB for the presence of proinsulin or GRP94, respectively. *B* and *C*: Representative blot of $n = 3$. IP, immunoprecipitation.

Next, analysis of secretory granules by transmission electron microscopy (EM) showed that vesicles in GRP94 KD cells had a bigger mean diameter (349 nm in GRP94 KD vs. 212 nm in controls) and an increased number of granules with lower mean density (Fig. 4*C* and *D*). In control cells, there was a positive correlation between

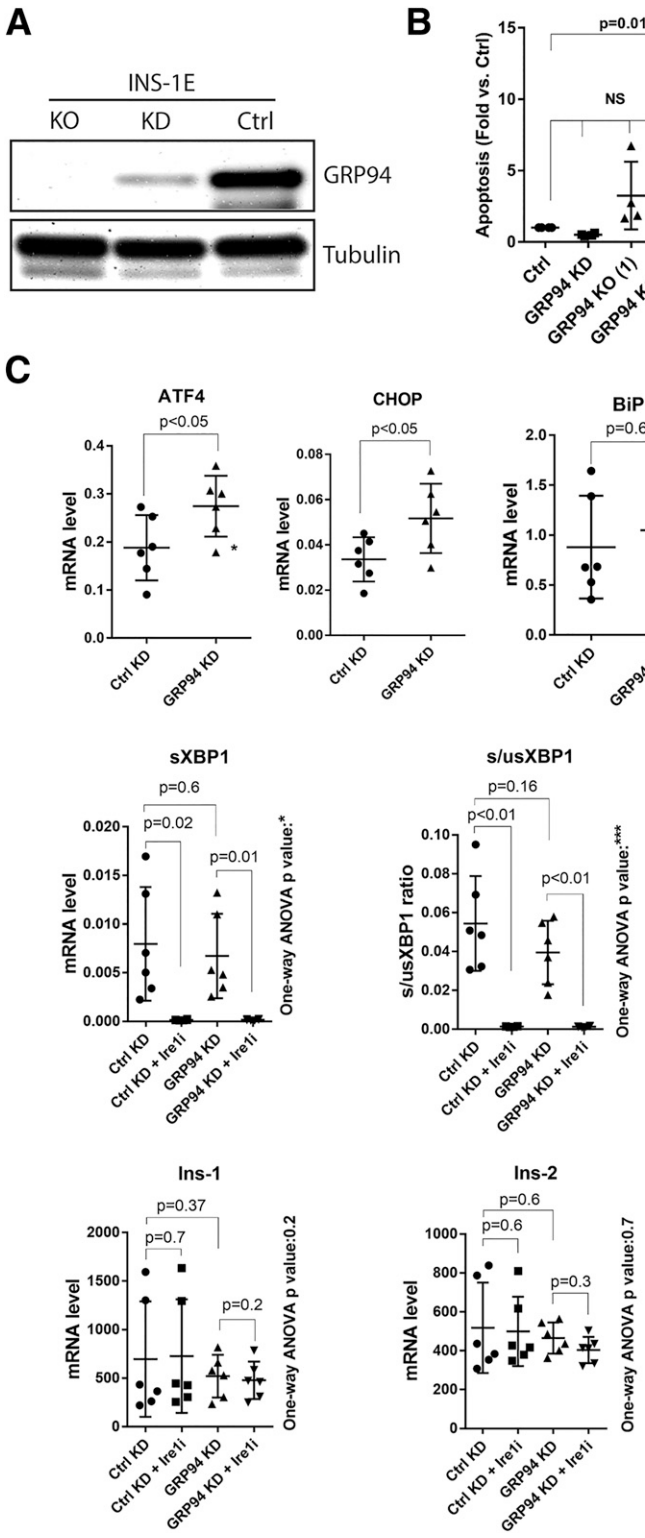

Figure 2—GRP94 KD or KO does not lead to β-cell death and induces ER stress via the PERK-ATF4-CHOP pathway. *A*: SDS-PAGE and WB analysis of GRP94 expression levels in INS-1E cells after lentiviral transduction with GRP94 targeting shRNA (cells lysed 2 weeks after viral transduction, KD) or CRISPR/Cas9 guide GRP94-directed RNA (clonal cell line shown 3 months after viral transduction, KO); $n = 5$. *B*: Apoptosis levels (representing internucleosomal degradation of genomic DNA) were analyzed in GRP94 KD and KO (clone 1 and 2) and control cells exposed for 24 h to 1 μmol/L of thapsigargin (Tg); $n = 4$. *C*: mRNA levels of ER stress pathways and Ins-1/2 genes were analyzed by quantitative RT-PCR in INS-1E control and GRP94 KD cells. The Ire1 inhibitor 4q8C (Ire1i) was used at 30 μmol/L for 4 h. Data represent the means ± SD analyzed by Bonferroni-corrected paired Student *t* test of treatments vs. control, $^*P < 0.02$; $^{***}P < 0.0005$; $n = 6$. Ctrl, control.

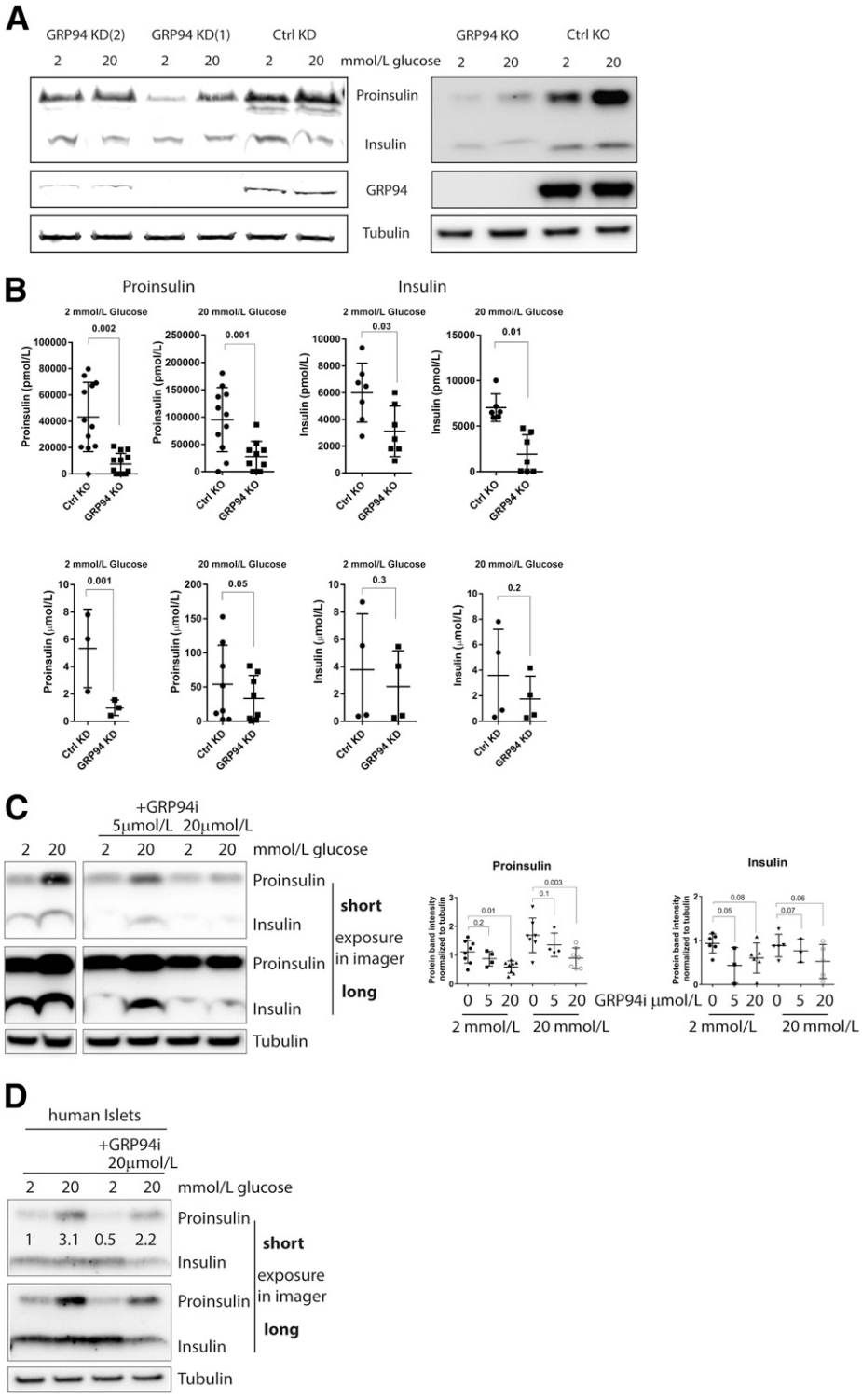

Figure 3—Diminished intracellular proinsulin and insulin contents after GRP94 KD, KO, or pharmacological inhibition. SDS-PAGE and WB (*A*, *C*, and *D*) or ELISA (300,000 cells) (*B*) analysis of proinsulin and insulin expression levels in INS-1E cells and dispersed human islet cells (n = 2) (*D*) after 3 h in 2 or 20 mmol/L glucose–containing media after lentiviral transduction of GRP94-specific shRNA (cells collected 2 weeks after viral transduction, KD [shGRP94 1 and 2]), CRISPR/Cas9 guide GRP94-directed RNA (clonal cell lines shown 3 months after viral transduction, KO), and 4-h exposure to GRP94-specific ATPase inhibitor PU-WS13 (representative blot of n = 6 on the left and band quantification on the right). Data represent means ± SD analyzed by Bonferroni-corrected paired Student *t* test of treatments vs. control. Ctrl, control.

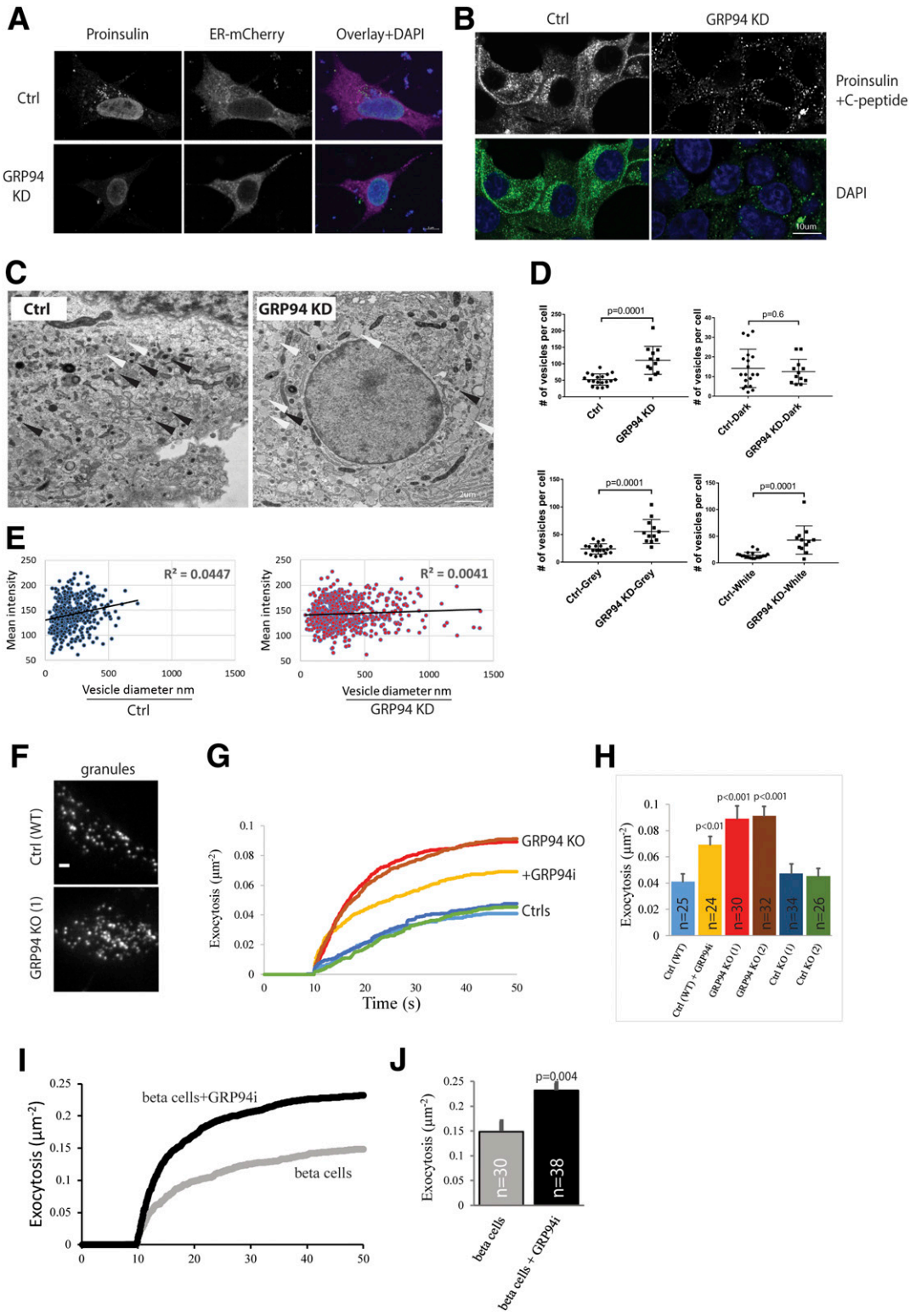

Figure 4—GRP94 KD cells show diminished, non-ER proinsulin staining accompanied by an increased number of larger secretory granules with amorphic content and increased exocytotic events. *A*: INS-1E cells (control [Ctrl] or GRP94 KD) were transfected with plasmids encoding for ER-mCherry, and 48 h later, cells were incubated for 3 h in 2 mmol/L glucose–containing medium. Next, cells were fixed with 2% paraformaldehyde and immunostained with mouse monoclonal antiproinsulin (GS-9A8) antibody followed by secondary antibody treatment (FITC). *B*: GRINCH cells were clonally derived from an INS-1 cell line stably expressing hProCpepSfGFP. The cells were incubated for 3 h in 2 mmol/L glucose–containing medium and fixed with 2% paraformaldehyde. *A* and *B*: Immunofluorescence was acquired by confocal laser microscopy, and illustrative images from three independent experiments are shown. *C*: Representative transmission EM of Ctrl and GRP94 KD INS-1E cells cultured for 3 h in 2 mmol/L glucose–containing medium. Images were obtained using a CM100 BioTWIN with tungsten emitter. Arrows point to secretory vesicles (black, vesicles with dark content; white, vesicles with gray/white content). *D* and *E*: EM-visualized vesicles were manually counted,

granule size and density, which was lacking in GRP94 KD cells (Fig. 4*E*). The higher number of granules was paralleled by accelerated K^+-stimulated exocytosis of fluorescently labeled granules in GRP94 KO cells, GRP94i-pretreated wild-type INS-1E cells, and human islets (Fig. 4*F–J* and Supplementary Videos 1 and 2). The density of labeled granules at the plasma membrane was similar for all cells and conditions (Supplementary Fig. 8), and granule docking was not affected. Immunogold staining of secretory granules for mature insulin in GRP94 KO and GRP94i-pretreated cells indicated a 30–60% reduction of granules containing immunogold particles and an increase in granules with no staining, as compared with control cells (Table 1).

Table 1—GRP94 KO and GRP94 ATPase inhibition lead to diminished content of mature insulin in secretory granules

Number of insulin molecules detected	Control	GRP94i	GRP94 KO
0	68	84	78.5
1–2	22	10	15.5
3–4	9.7	5.4	5.8
5 and more	11.7	8.4	5.5

Data represent the percentage of each category of stained vesicles vs. all vesicles counted in a given experimental condition.

Proinsulin Processing Is Modified and Proinsulin Half-Life Shortened in GRP94 KD/KO Cells

Under nonreducing conditions in steady state at 2 mmol/L glucose, significantly diminished levels of proinsulin conversion intermediates and mature insulin (Fig. 5*A*) in GRP94 KD versus control were observed. To gain insight into the proinsulin post-ER processing, we performed pulse-chase labeling. Cells were labeled for 1 h and chased for 1 h. Proinsulin is cleaved by endoproteases PC1/3 and PC2, resulting in the formation of four proinsulin conversion intermediates (29). They have the molecular weight of proinsulin, but their hydrodynamic radius is larger, resulting in a slower migration under nonreducing conditions. Indeed, we observed four proinsulin conversion intermediates in control cells, but their relative abundance in GRP94 KD/KO cells was different, indicating that GRP94 deficiency modified processing via endoproteases (bands 1–4 in Fig. 5*B*).

Since Ins-1/2 mRNA levels and proinsulin biosynthesis were comparable between control and GRP94 KD cells (Figs. 2*C* and 5*B*), but steady-state proinsulin levels were lower in GRP94 KD/KO cells, we reasoned that proinsulin misprocessing in ER or post-ER compartments results in either increased secretion or degradation, resulting in shortened intracellular protein half-life. In fact, upon inhibition of protein synthesis with 100 μmol/L cycloheximide, proinsulin was reduced by 50% after 30 min in GRP94 KD lysates versus 1–3 h in control cell lysates (Fig. 5*C*), demonstrating a shorter proinsulin protein half-life in GRP94 KD cells. To examine if the shorter half-life could be accounted for by increased secretion (INS-1E cells secrete small amounts of proinsulin even at 2 mmol/L glucose) (Supplementary Fig. 9*A*), we pretreated cells with 200 nmol/L of brefeldin A, inhibiting ER-Golgi anterograde transport before cycloheximide exposure. This efficiently inhibited proinsulin secretion (Supplementary Fig. 9*A*), whereas the proinsulin half-life still differed substantially between cell types (1–2 h in GRP94 KD/KO vs. ~4 h in control cells) (Fig. 5*D*). Finally, treatment with brefeldin A for 4 h did not restore intracellular levels of proinsulin in GRP94 KO and GRP94i-treated cells (Supplementary Fig. 9*B–E*). Taken together, these data indicate that the shorter half-life is likely caused by enhanced proinsulin degradation by ER-associated degradation via the proteasome.

Glucose-Stimulated Insulin Secretion Is Impaired in the GRP94-Deficient Cells

We anticipated that GRP94 activity–related changes in proinsulin-insulin processing would lead to lower secretion of mature insulin during glucose-stimulated insulin secretion. Indeed, INS-1E control cells increased insulin secretion two- to threefold in response to glucose stimulation, but this was not the case for GRP94 KD or cells pretreated for 24 h with 20 μmol/L of GRP94i (Fig. 6*A* and *B*, left panels). Neither control nor GRP94 KD/GRP94i cells increased their basal proinsulin secretion (Fig. 6*A* and *B*, right panels). We confirmed the inhibition of glucose-stimulated mature insulin secretion in dispersed human islet cells transduced with lentivirus carrying GRP94-targeting shRNA (Fig. 6*C*). Similarly, glucose-stimulated insulin and proinsulin secretion over 6 h was markedly lower in GRP94 KO/GRP94i compared with control cells (Fig. 6*D*).

To test if GPR94 inhibition induced changes in the biological activity of secreted insulin, we compared the

marked, and measured in 19 images of Ctrl and 12 images of GRP94 KD cells. In total, 427 vesicles for Ctrl and 618 for GRP94 KD cells were analyzed. Each dot on the graph represents the number of vesicles in a single cell (*D*) (data represent the means ± SEM analyzed by Bonferroni-corrected nonpaired Student *t* test of treatments vs. Ctrl). Mean signal intensity of vesicles: dark <145, gray 146–170, and white >171. Correlation between vesicle size and intensity signal of its content in Ctrl and GRP94 KD cells (*E*). *C–E*: $n = 3$. *F–J*: Exocytosis of fluorescently labeled granules during application of 75 mmol/L K^+. *F*: Representative TIRF microscopy images of Ctrl (WT) and GRP94 KO (1) INS-1 cells expressing the granule marker NPY-GFP. *G*: Average cumulative number of exocytotic events as a function of time and normalized to the cell area; K^+ was elevated from 10 s. INS-1E (Ctrl), GRP94 KO, and GRP94i (20 μmol/L for 24 h). *H*: Total exocytosis (mean ± SEM) for three independent experiments as in *I*; number of cells is shown on bars. *I* and *J*: As in *G* and *H*, but for human β-cells from five donors with or without GRP94i pretreatment (20 μmol/L for 24 h). In *H* and *J*, the difference from Ctrl was tested with Student *t* tests.

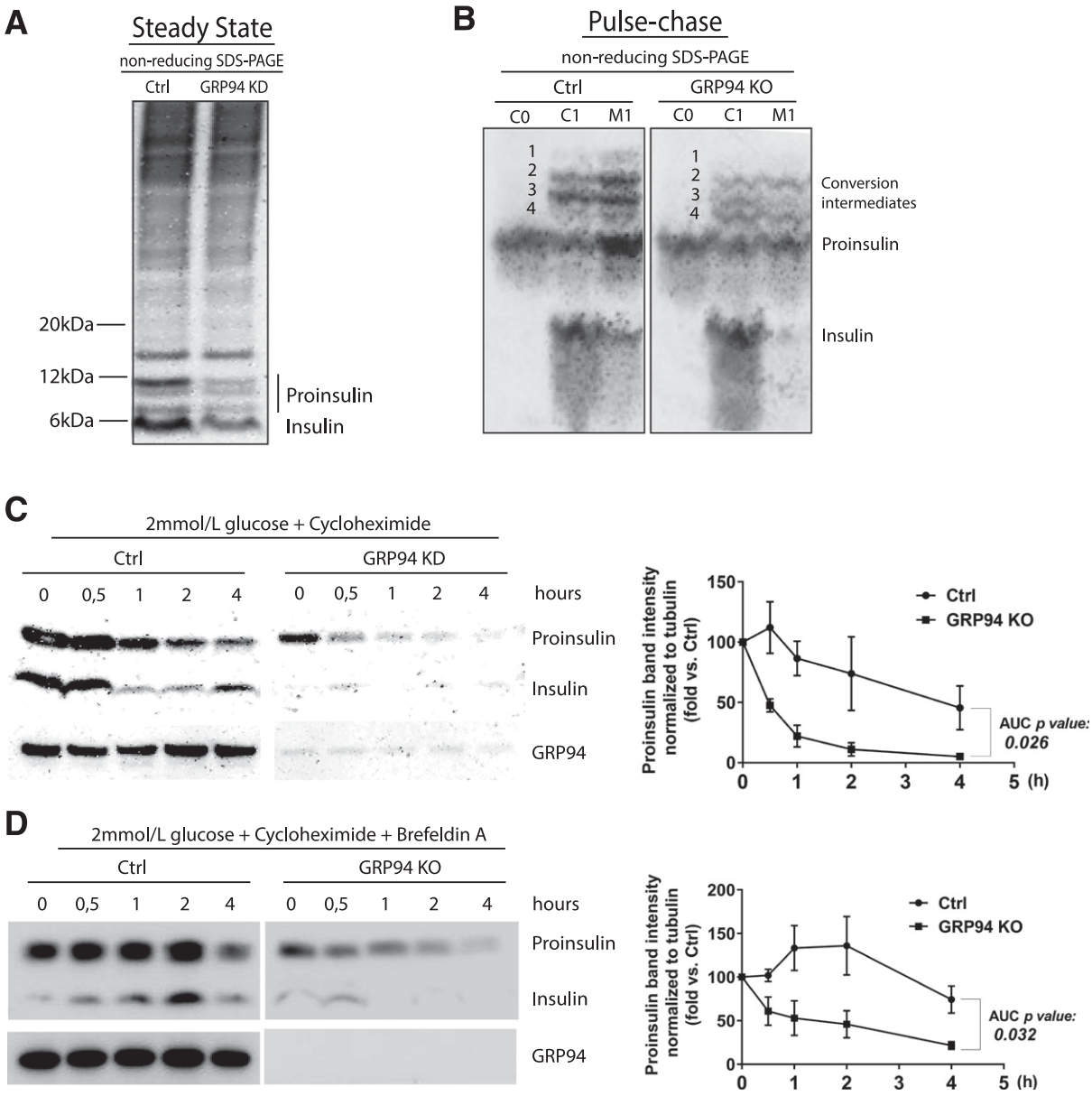

Figure 5— GRP94 KD/KO causes proinsulin misprocessing and increased cellular turnover. *A*: Control (Ctrl) and GRP94 KD INS-1E cells were cultured for 3 h in 2 mmol/L glucose containing Krebs-Ringer bicarbonate HEPES (KRBH) buffer and lysed. In order to preserve intramolecular disulfide bonds and visualize proinsulin folding intermediates, cell lysates were analyzed by nonreducing SDS-PAGE (Nu-Page 4–12% Bis-Tris Protein Gel), and proinsulin and insulin were visualized through WB with antiproinsulin and anti-insulin antibody (L6B10; Cell Signaling); $n = 3$. *B*: INS-1E Ctrl or GRP94 KO cells were pulse labeled with ^{35}S-Met/Cys for 1 h (C0) and chased for 1 h (C1 and M1) in 11 mmol/L glucose. Cell lysates and culture supernatants were immunoprecipitated with anti-insulin antibody, and newly synthesized proinsulin was analyzed by nonreducing Tris-tricine-urea SDS-PAGE and phosphorimaging. Numbers 1–4 identify proinsulin 1 and 2 conversion intermediates. C, cells; M, media. $n = 3$. *C*: INS-1E Ctrl and GRP94 KD cells were cultured for 3 h in 2 mmol/L glucose–containing KRBH buffer, and subsequently 100 μmol/L of the protein synthesis inhibitor cycloheximide was added and cells were lysed at the indicated time points; $n = 3$. *D*: Ctrl and GRP94 KO cells were treated similarly, but 200 nmol/L of the inhibitor of exocytosis brefeldin A was added to the culture media from the start of the experiment. Cell lysates were analyzed via reducing SDS-PAGE, and proinsulin and insulin were visualized through WB with antiproinsulin antibody; $n = 3$. Quantification of proinsulin bands was performed with ImageJ and normalized to tubulin bands (*C* and *D*, right panels). The quantification data are presented as means ± SEM analyzed by Bonferroni-corrected paired Student *t* test of treatments vs. Ctrl. AUC, area under the curve.

ability of endogenously released and externally applied insulin to activate insulin receptors in MIN6 β-cells by recording the changes of plasma membrane PIP3 that follows insulin-triggered activation of PI3 kinase (30). Whereas the PIP3 response to K^+-triggered insulin secretion was reduced after treatment with GRP94i, the response to 100 nmol/L exogenous insulin was unaffected (Fig. 6*E*). Accordingly, the ratio of K^+ over insulin-triggered PIP3 formation was lower (Fig. 6*F*, left) and the time to half-maximum K^+-induced PIP3 increase was prolonged

(Fig. 6*F*, right) in GRP94i-treated cells, consistent with reduced amounts and/or diminished bioactivity of secreted insulin.

GRP94 mRNA Is Overexpressed in Islets From Patients With T2D

Since the increased demand for insulin in T2D may require compensatory upregulation of a chaperone responsible for proinsulin folding, we analyzed single-cell sequencing of dispersed islets derived from four deceased patients with T2D and six control subjects (EBI accession no. MTAB-5061). The results demonstrated significant upregulation of *grp94* in β- and δ-cells but not in α-cells of patients with T2D (Fig. 6*F*); however, these data have not been independently validated (e.g., by quantitative PCR).

DISCUSSION

Characterization of mechanisms regulating proinsulin folding and maturation to insulin, including the role of ER protein chaperones in this process, may reveal novel therapeutic targets to improve insulin secretory capacity and limit the progression of diabetes. It has been suggested that approximately one-third of wild-type proteins fail to fold properly (31). In the ER, this creates a pool of misfolded forms that are dealt with by UPR to maintain homeostatic balance in a healthy cell. Due to the lack of specific experimental models of misfolding or misprocessing of wild-type proinsulin, studies so far have focused on dissecting the handling of mutated proinsulin (32). Here, we discovered a novel role of a major ER luminal chaperone, GRP94, in the handling of the wild-type proinsulin. We found that GRP94 physically interacts with wild-type proinsulin, and β-cells with GRP94 deficiency or functional inhibition exhibit shorter proinsulin half-life, diminished intracellular proinsulin and insulin levels, post-ER misprocessing, an increased number of amorphic secretory granules with lower insulin content, reduced insulin bioactivity and secretion, and, finally, GRP94 overexpression in β-cells of patients with T2D as a likely compensatory response to increased proinsulin biosynthetic demand.

Since IGFs and proinsulin have similar tertiary structures and folding intermediates (21), we analyzed in silico GRP94-proinsulin interactions. The predicted proinsulin docking site (Fig. 1*A*) is in agreement with the GRP94 CBS localized within its COOH-terminal domain (33). The precise mode of GRP94 client folding is unknown, but the recently published GRP94 crystal structure (34) identifies a peptide-binding channel formed by the GRP94 dimer that contains the COOH-terminal domain residues identified here to bind proinsulin within its chain A residues 73–83 in top prediction models.

After demonstrating that GRP94 or proinsulin immunoprecipitates contain proinsulin and GRP94, respectively (Fig. 1*B* and *C*), we induced GRP94 functional deficiency via GRP94-ATPase inhibition or protein KD or KO in model β-cells (Figs. 2*A* and 3*C*). All three approaches demonstrated a consistent phenotype of lower proinsulin and insulin cellular contents (Fig. 3). Induction of this phenotype is rapid in that changes in proinsulin levels were detected within 2 h after application of GRP94-ATPase inhibitor, indicating that GRP94 does not merely serve as a scaffold for proinsulin, but that its ATP turnover is linked to conformational changes critical for proinsulin folding and/or processing (as is the case for IGF-1/2) (35). The phenotype is also stable, as shown by the continuously low proinsulin levels in weeks (KD) and months (KO) of cultured β-cells.

Models of mutated proinsulin indicate that proinsulin misfolded in the ER leads to β-cell stress and apoptosis, insulin deficiency, and the onset of diabetes (32). In contrast, GRP94 KD/KO in β-cells led to a specific loss of proinsulin in the presence of ER stress that was limited to the PERK pathway, with no induction of the RIDD complex, no increase in apoptosis, and no other detrimental effects. How do we reconcile those two observations?

First, GRP94 deficiency has been shown to induce restricted cellular phenotypes. GRP94 KD in mouse embryo 10T1/2 cells induces limited ER stress and UPR response involving upregulation of BiP and PDIA6 only, in contrast to much broader responses to, e.g., BiP KD (15). Furthermore, animal models of tissue-specific GRP94 KO have phenotypes mostly limited to impaired function of the GRP94-dependent client of the tissue in question (GRP94 KO in muscle mimicking IGF-1 deficiency) (16) with otherwise restricted effects on cellular stress and viability.

Second, it can be argued that a GRP94 functional deficiency constitutes a more physiological model, where β-cell ER resources are insufficient to fulfill proinsulin production–related functions but at the same time are capable of efficiently disposing of wild-type proinsulin that cannot progress to the Golgi.

Proinsulin folding in the ER includes the formation of intramolecular disulfide bonds (36); from that perspective, we found no evidence that proinsulin in GRP94-deficient cells is improperly folded. However, in GRP94 KD cells, the steady-state level of proinsulin is low (Fig. 3*A* and *B*), suggesting that GRP94 presence is necessary for proinsulin stability shortly after its biosynthesis. Indeed, GRP94 is associated with ArsA arsenite transporter ATP-binding homolog 1 (ASNA1) (37), a protein that is required for the posttranslational delivery of preproinsulin to the ER (38,39).

GRP94 KD/KO results in a substantially shorter proinsulin half-life, indicating increased, likely active, degradation (Fig. 5*C* and *D*). At the same time, a limited amount of proinsulin is folded and transported to the Golgi, where its processing appears altered (Fig. 5*B*). Since GRP94 promotes heterodimer formation (40), a possible explanation of our observations is perturbed proinsulin dimerization, and subsequent misprocessing and packaging. After monomer folding, proinsulin dimerizes in the ER, followed by formation of hexamers around Zn^{2+} in the Golgi (41,42) and final cleavages conveyed by peptidases (29,43), converting proinsulin to mature insulin and C-peptide. Under physiological conditions, four proinsulin

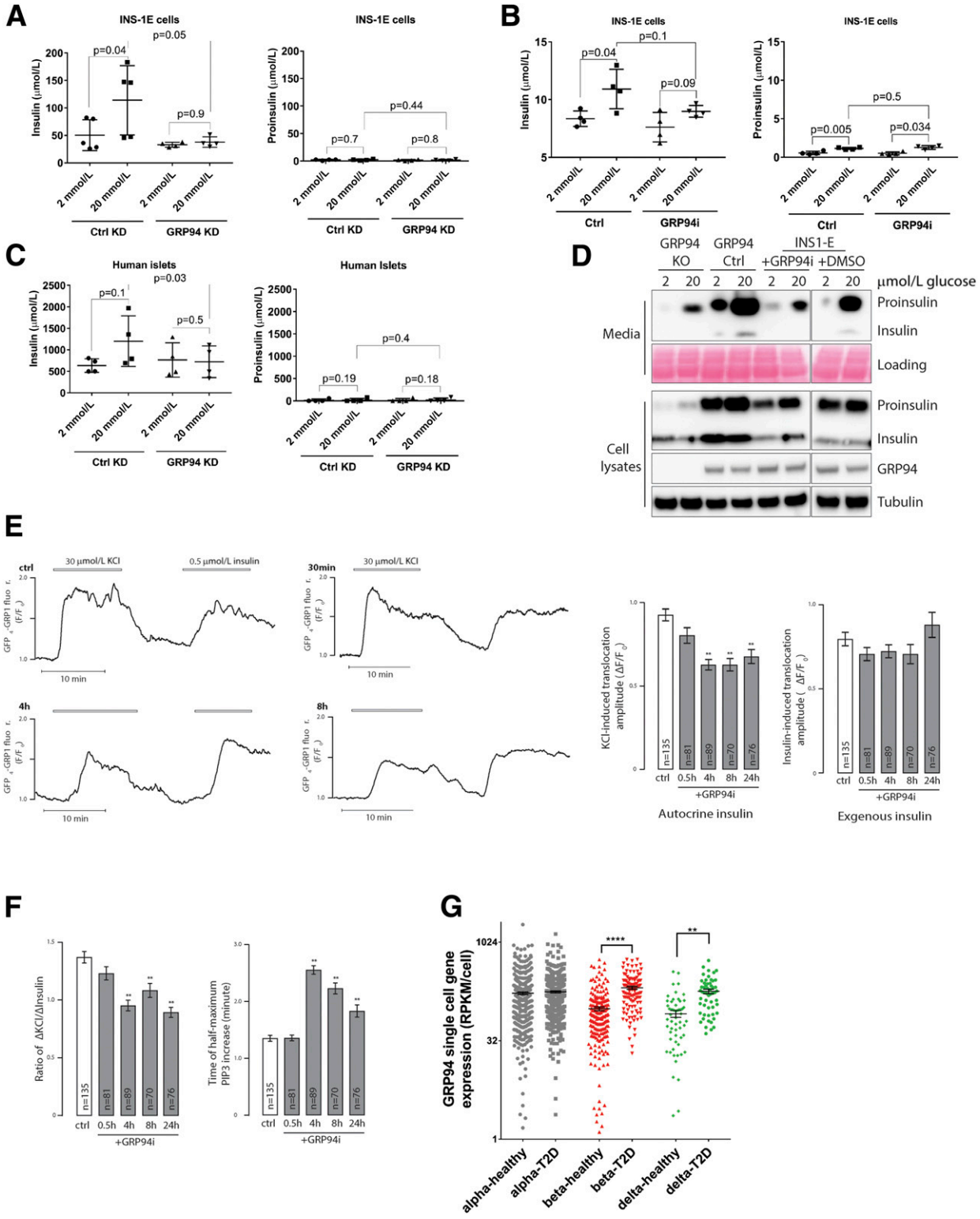

Figure 6—Glucose-stimulated secretion of bioactive insulin is impaired in GRP94-deficient cells, and GRP94 mRNA is overexpressed in islet cells from patients with T2D. INS-1E control (Ctrl) and GRP94 KD or INS-1E cells exposed to 20 μmol/L of GRP94i for 24 h (*A* [$n = 5$] and *B* [$n = 4$]) as well as dispersed human islet cells (*C*) (1 week after transduction with lentivirus carrying nontargeting or GRP94-targeting shRNA coding plasmids; $n = 4$) were tested for their ability to secrete insulin in response to the given glucose concentrations in Krebs-Ringer bicarbonate HEPES buffer. Supernatants were analyzed by ELISAs specifically detecting mature insulin (*A–C*, left graphs) or proinsulin (*A–C*, right graphs) only. The bars represent the means ± SD. *D*: Accumulated secretion of proinsulin and insulin over the period of 6 h in INS-1E Ctrl and 20 μmol/L GRP94i 24 h pretreated, GRP94 KO Ctrl, and KO cells were analyzed by SDS-PAGE and WB ($n = 3$). One milliliter of cell supernatants was concentrated using 10-kDa molecular weight cutoff filters to remove salts and reduce volume to 15 μL. *E* and *F*: TIRF recordings of PIP3 from a single MIN6 cell stimulated with 30 mmol/L K^+ and 0.5 μmol/L insulin. Cells were preincubated without or with 20 μmol/L of the GRP94i for 0.5, 4, or 8 h. *F*: Means ± SEM of the amplitudes of the PIP3 responses to endogenous K^+-triggered insulin

conversion intermediates are observed (originating from rodent insulin 1 and 2). In our control cells, two intermediates were most abundant, with clear change in their relative abundance in GRP94 KO cells (Fig. 5*B*). This could reflect *1*) altered physiological structural constraints of proinsulin for efficient processing by endoproteases or *2*) altered composition of peptidases, which themselves could be GRP94 folding substrates. However, treatment of GRP94-deficient cells with the ER-Golgi anterograde transport inhibitor brefeldin A did not restore proinsulin content or extend its half-life to control levels (Fig. 5*D* and Supplementary Fig. 9). This indicates that the major loss of proinsulin in GRP94 KD/KO occurs at the level of the ER, probably involving proinsulin retro-translocation from the ER into cytosol and proteasome-dependent degradation (44), but is not a consequence of post-ER misprocessing.

The physiological conversion of proinsulin to insulin decreases the solubility of the insulin hexamer (45), leading to crystallization, visualized as the dense granule core. GRP94-deficient cells contained a higher number of larger granules with amorphous cargo (no dense core), and the correlation between their size and content was lost (Fig. 4*E*). Additionally, granule immunogold staining for insulin indicates a reduction in mature insulin content (Table 1), with an autocrine bioactivity test (Fig. 6*E* and *F*) further demonstrating that less bioactive insulin is secreted from GRP94-deficient cells. These observations do not reflect an effect of GRP94 on granule biogenesis or docking, since granule density at the plasma membrane evaluated by NPY-GFP labeling was unaffected (Supplementary Fig. 8). Interestingly, GRP94 KD/KO cells exhibit impaired glucose-stimulated insulin secretion (Fig. 6*A*–*C*) even though they contain a higher number of granules that undergo increased exocytosis (Fig. 4*C*–*J*). It seems plausible that proinsulin exiting the ER does not get condensed efficiently in the GRP94 KO cells, resulting in the production of more and bigger granules, since by remaining uncondensed, the proinsulin needs more volume to be packed. Furthermore, one could speculate that granules in the GRP94 KO are on average younger because they are more likely to be removed by auto/crinophagy, and younger granules are more fusogenic than their older counterparts (46). A similar mismatch between secretion and exocytotic events has been observed in chromogranin B–deficient cells (47).

Our results point to a functional link between GRP94 activity and the amount of secreted insulin. By inference, one would expect compensatory induction in GRP94 expression in conditions where a higher production of insulin is required (e.g., T2D). Indeed, single-cell sequencing of islet cells from human donors with T2D demonstrated upregulation of GRP94 mRNA in β- and δ- but not α-cells (Fig. 6*G*). Interestingly, δ-cells express the highest IGF-1 levels in the endocrine pancreas (IGF-1 is a client of GRP94) (48,49), and IGF-1 may contribute to maintain or even increase β-cell mass to further compensate for insulin requirements in T2D.

Recently, GRP94 has been shown to be essential for β-cell development in that β-cell–specific GRP94 KO mice exhibit pancreatic hypoplasia and reduced β-cell proliferation and mass (20). These mice remained euglycemic but had impaired glucose tolerance, reduced serum insulin and insulin mRNA expression at embryonic day 14.5, an increased number of amorphous secretory granules (nonquantified), and distended ER in EM. These authors did not investigate putative GRP94 function in proinsulin handling, and their cellular model data are in stark contrast to our results and the author's own animal model. Their cellular model of GRP94 KD shows induction of Ins-1/2 mRNA expression, increased insulin content, and increased basal and glucose-induced insulin secretion. These major discrepancies may arise from an off-target effect of single position–directed shRNA used repeatedly on consecutive days. Further studies of inducible β-cell–specific GRP94 KO mice and a broader use of β-cell cellular models, human islets, and GRP94-specific small molecule inhibitors are needed.

In summary, our study has established, for the first time, the importance of GRP94 as an essential molecular chaperone in proinsulin handling in pancreatic β-cells. It highlights a key function for GRP94 not in the most obvious context of ER stress regulation but rather as a chaperone with client-specific phenotypes. As such, our findings create a novel platform guiding further investigations to dissect pathways relevant for wild-type proinsulin processing in the physiological and pathophysiological context and identification of novel therapeutics targeting proinsulin handling.

Acknowledgments. The authors greatly appreciate the European Consortium for Islet Transplantation (Milan, Italy) and the Nordic Network for Clinical Islet Transplantation (Uppsala, Sweden) for providing human islets. The authors acknowledge the valuable assistance from the Core Facility for Integrated Microscopy, Faculty of Health and Medical Sciences, University of Copenhagen.

secretion (left) and exogenous insulin (right) from experiments as in *E* with the indicated treatments and numbers of cells. $^{**}P < 0.01$ for difference from Ctrl (one-way ANOVA with post hoc Tukey honestly significant difference test). Means ± SEM for the ratio of the PIP3 amplitude in response to K^+ over that of insulin in individual cells (right). *F*: Means ± SEM for the time to half-maximal PIP3 increase after K^+ stimulation. $^{**}P < 0.01$ for difference from Ctrl (one-way ANOVA with post hoc Tukey honestly significant difference test). *G*: Expression levels of GRP94 in dispersed donor human islets α- and β-cells from healthy individuals ($n = 6$) and patients with T2D ($n = 4$) were determined by single-cell RNA sequencing and quantified by expression values per cell. Statistical analysis was performed using ANOVA with Bonferroni correction for multiple comparisons of T2D vs. healthy donors. $^{**}P < 0.01$; $^{****}P < 0.0001$.

The authors also thank C. Wollheim and P. Maechler (University Medical Centre, Geneva, Switzerland) for sharing the rat insulinoma INS-1E cell line as well as Y. Argon (Children's Hospital of Philadelphia, Philadelphia, PA) for sharing the cGRP94-GFP coding plasmid.

Funding. This project was funded by Zealand Pharma A/S (S.M.G.); the Danish Diabetes Academy (S.M.G. and T.D.); the Department of Biomedical Sciences at the University of Copenhagen (S.M.G., T.D., and M.T.M.); the Augustinus Foundation (T.D. and M.T.M.); The Punjab Educational Endowment Fund, Pakistan (M.S.K.); the Swedish Research Council, Diabetesfonden (Sweden), Family Ernfors Foundation, and the Novo Nordisk Foundation (S.B. and A.T.); the National Institutes of Health (DK48280 to P.A.); and the Danish Council for Independent Research (DFF-4092-00066), Dagmar Marshall Foundation, A.P. Møller Foundation, Kirsten and Freddy Johansen Foundation, and Eva and Hans Carl Holm Foundation (M.T.M.)

Duality of Interest. No potential conflicts of interest relevant to this article were reported.

Author Contributions. S.M.G. and T.D. developed the protocols for the experiments, conducted experiments, performed the statistical analysis, constructed figures and tables (Figs. 2, 3, 5, and 6), and actively participated in writing and reviewing the manuscript. C.H.A. (Fig. 3), S.P. (Figs. 1 and 6), M.O.-H. (Fig. 4), M.Y., M.S.K., and O.C. (Fig. 6), S.E.B. (Fig. 1 and Supplementary Fig. 1 and Table 3), K.K. (Figs. 2, 3, and 5), and C.Pi. (Fig. 3 and Supplementary Fig. 7) conducted experiments and performed the statistical analysis. L.H. and P.A. (Fig. 5) developed the protocols, conducted experiments, and actively participated in critical data analysis and writing the manuscript. C.Pr. and M.J.P. (Figs. 4 and 6) developed the protocols, conducted experiments, and participated in critical data analysis and writing the manuscript. B.T. (Fig. 6) conducted bioinformatics analysis of single-cell RNA sequencing data. S.B., A.T., and T.M.-P., developed the protocols for the experiments, provided experimental tools, and participated in critical data analysis and writing the manuscript. M.T.M. initiated the study and was the lead supervisor, developed the protocols for the experiments, conducted experiments, performed the statistical analysis, constructed figures and tables, and wrote the manuscript. M.T.M. is the guarantor of this work and, as such, had full access to all the data in the study and takes responsibility for the integrity of the data and the accuracy of the data analysis.

References

1. Scheuner D, Kaufman RJ. The unfolded protein response: a pathway that links insulin demand with beta-cell failure and diabetes. Endocr Rev 2008;29:317–333

2. Rubenstein AH, Melani F, Pilkis S, Steiner DF. Proinsulin. Secretion, metabolism, immunological and biological properties. Postgrad Med J 1969;45 (Suppl.):476–481

3. Liu M, Lara-Lemus R, Shan SO, et al. Impaired cleavage of preproinsulin signal peptide linked to autosomal-dominant diabetes. Diabetes 2012;61:828–837

4. Winter J, Klappa P, Freedman RB, Lilie H, Rudolph R. Catalytic activity and chaperone function of human protein-disulfide isomerase are required for the efficient refolding of proinsulin. J Biol Chem 2002;277:310–317

5. Goodge KA, Hutton JC. Translational regulation of proinsulin biosynthesis and proinsulin conversion in the pancreatic beta-cell. Semin Cell Dev Biol 2000; 11:235–242

6. Liu M, Li Y, Cavener D, Arvan P. Proinsulin disulfide maturation and misfolding in the endoplasmic reticulum. J Biol Chem 2005;280:13209–13212

7. Marzec M, Eletto D, Argon Y. GRP94: an HSP90-like protein specialized for protein folding and quality control in the endoplasmic reticulum. Biochim Biophys Acta 2012;1823:774–787

8. Eletto D, Dersh D, Argon Y. GRP94 in ER quality control and stress responses. Semin Cell Dev Biol 2010;21:479–485

9. Staron M, Yang Y, Liu B, et al. gp96, an endoplasmic reticulum master chaperone for integrins and Toll-like receptors, selectively regulates early T and B lymphopoiesis. Blood 2010;115:2380–2390

10. Yang Y, Liu B, Dai J, et al. Heat shock protein gp96 is a master chaperone for toll-like receptors and is important in the innate function of macrophages. Immunity 2007;26:215–226

11. Wanderling S, Simen BB, Ostrovsky O, et al. GRP94 is essential for mesoderm induction and muscle development because it regulates insulin-like growth factor secretion. Mol Biol Cell 2007;18:3764–3775

12. Chang SC, Erwin AE, Lee AS. Glucose-regulated protein (GRP94 and GRP78) genes share common regulatory domains and are coordinately regulated by common trans-acting factors. Mol Cell Biol 1989;9:2153–2162

13. Mao C, Wang M, Luo B, et al. Targeted mutation of the mouse Grp94 gene disrupts development and perturbs endoplasmic reticulum stress signaling. PLoS One 2010;5:e10852

14. Paris S, Denis H, Delaive E, et al. Up-regulation of 94-kDa glucose-regulated protein by hypoxia-inducible factor-1 in human endothelial cells in response to hypoxia. FEBS Lett 2005;579:105–114

15. Eletto D, Maganty A, Eletto D, et al. Limitation of individual folding resources in the ER leads to outcomes distinct from the unfolded protein response. J Cell Sci 2012;125:4865–4875

16. Barton ER, Park S, James JK, et al. Deletion of muscle GRP94 impairs both muscle and body growth by inhibiting local IGF production. FASEB J 2012;26: 3691–3702

17. Dollins DE, Warren JJ, Immormino RM, Gewirth DT. Structures of GRP94-nucleotide complexes reveal mechanistic differences between the hsp90 chaperones. Mol Cell 2007;28:41–56

18. Schulte TW, Akinaga S, Murakata T, et al. Interaction of radicicol with members of the heat shock protein 90 family of molecular chaperones. Mol Endocrinol 1999;13:1435–1448

19. Patel PD, Yan P, Seidler PM, et al. Paralog-selective Hsp90 inhibitors define tumor-specific regulation of HER2. Nat Chem Biol 2013;9:677–684

20. Kim DS, Song L, Wang J, et al. GRP94 is an essential regulator of pancreatic β-cell development, mass, and function in male mice. Endocrinology 2018;159: 1062–1073

21. Rinderknecht E, Humbel RE. The amino acid sequence of human insulin-like growth factor I and its structural homology with proinsulin. J Biol Chem 1978;253: 2769–2776

22. Haataja L, Snapp E, Wright J, et al. Proinsulin intermolecular interactions during secretory trafficking in pancreatic β cells. J Biol Chem 2013;288:1896–1906

23. Ghiasi SM, Krogh N, Tyrberg B, Mandrup-Poulsen T. The No-Go and nonsense-mediated RNA decay pathways are regulated by inflammatory cytokines in insulin-producing cells and human islets and determine β-cell insulin biosynthesis and survival. Diabetes 2018;67:2019–2037

24. Segerstolpe Å, Palasantza A, Eliasson P, et al. Single-cell transcriptome profiling of human pancreatic islets in health and type 2 diabetes. Cell Metab 2016; 24:593–607

25. Berman HM, Westbrook J, Feng Z, et al. The protein data bank. Nucleic Acids Res 2000;28:235–242

26. Ostrovsky O, Ahmed NT, Argon Y. The chaperone activity of GRP94 toward insulin-like growth factor II is necessary for the stress response to serum deprivation. Mol Biol Cell 2009;20:1855–1864

27. Harding HP, Novoa I, Zhang Y, et al. Regulated translation initiation controls stress-induced gene expression in mammalian cells. Mol Cell 2000; 6:1099–1108

28. Han D, Lerner AG, Vande Walle L, et al. IRE1alpha kinase activation modes control alternate endoribonuclease outputs to determine divergent cell fates. Cell 2009;138:562–575

29. Rhodes CJ, Lincoln B, Shoelson SE. Preferential cleavage of des-31,32-proinsulin over intact proinsulin by the insulin secretory granule type II endopeptidase. Implication of a favored route for prohormone processing. J Biol Chem 1992;267:22719–22727

30. Dyachok O, Idevall-Hagren O, Sågetorp J, et al. Glucose-induced cyclic AMP oscillations regulate pulsatile insulin secretion. Cell Metab 2008;8:26–37

31. Schubert U, Antón LC, Gibbs J, Norbury CC, Yewdell JW, Bennink JR. Rapid degradation of a large fraction of newly synthesized proteins by proteasomes. Nature 2000;404:770–774

32. Liu M, Wright J, Guo H, Xiong Y, Arvan P. Proinsulin entry and transit through the endoplasmic reticulum in pancreatic beta cells. Vitam Horm 2014;95:35–62
33. Wu S, Hong F, Gewirth D, Guo B, Liu B, Li Z. The molecular chaperone gp96/GRP94 interacts with Toll-like receptors and integrins via its C-terminal hydrophobic domain. J Biol Chem 2012;287:6735–6742
34. Huck JD, Que NL, Hong F, Li Z, Gewirth DT. Structural and functional analysis of GRP94 in the closed state reveals an essential role for the pre-N domain and a potential client-binding site. Cell Reports 2017;20:2800–2809
35. Ostrovsky O, Makarewich CA, Snapp EL, Argon Y. An essential role for ATP binding and hydrolysis in the chaperone activity of GRP94 in cells. Proc Natl Acad Sci U S A 2009;106:11600–11605
36. Haataja L, Manickam N, Soliman A, Tsai B, Liu M, Arvan P. Disulfide mispairing during proinsulin folding in the endoplasmic reticulum. Diabetes 2016;65:1050–1060
37. Natarajan B, Naredi P, Kao G. ENPL-1, a GRP94 homolog, interacts with ASNA-1 to promote insulin/IGF secretion in Caenorhabditis elegans [Internet], 2012. Available from http://urn.kb.se/resolve?urn=urn:nbn:se:umu:diva-60951. Accessed 13 April 2018
38. Stefanovic S, Hegde RS. Identification of a targeting factor for post-translational membrane protein insertion into the ER. Cell 2007;128:1147–1159
39. Kao G, Nordenson C, Still M, Rönnlund A, Tuck S, Naredi P. ASNA-1 positively regulates insulin secretion in *C. elegans* and mammalian cells. Cell 2007;128:577–587
40. Randow F, Seed B. Endoplasmic reticulum chaperone gp96 is required for innate immunity but not cell viability. Nat Cell Biol 2001;3:891–896
41. Frank BH, Veros AJ. Physical studies on proinsulin-association behavior and conformation in solution. Biochem Biophys Res Commun 1968;32:155–160
42. Dodson G, Steiner D. The role of assembly in insulin's biosynthesis. Curr Opin Struct Biol 1998;8:189–194
43. Davidson HW. (Pro)insulin processing: a historical perspective. Cell Biochem Biophys 2004;40(Suppl.):143–158
44. Hartley T, Siva M, Lai E, Teodoro T, Zhang L, Volchuk A. Endoplasmic reticulum stress response in an INS-1 pancreatic beta-cell line with inducible expression of a folding-deficient proinsulin. BMC Cell Biol 2010;11:59
45. Hill CP, Dauter Z, Dodson EJ, Dodson GG, Dunn MF. X-ray structure of an unusual Ca2+ site and the roles of Zn2+ and Ca2+ in the assembly, stability, and storage of the insulin hexamer. Biochemistry 1991;30:917–924
46. Müller A, Mziaut H, Neukam M, Knoch KP, Solimena M. A 4D view on insulin secretory granule turnover in the β-cell. Diabetes Obes Metab 2017;19(Suppl. 1): 107–114
47. Obermüller S, Calegari F, King A, et al. Defective secretion of islet hormones in chromogranin-B deficient mice. PLoS One 2010;5:e8936
48. Maake C, Reinecke M. Immunohistochemical localization of insulin-like growth factor 1 and 2 in the endocrine pancreas of rat, dog, and man, and their coexistence with classical islet hormones. Cell Tissue Res 1993;273:249–259
49. Pullen TJ, Huising MO, Rutter GA. Analysis of purified pancreatic islet beta and alpha cell transcriptomes reveals 11β-hydroxysteroid dehydrogenase (Hsd11b1) as a novel disallowed gene. Front Genet 2017;8:41